Surface freezing in binary mixtures of chain molecules. II. Dry and hydrated alcohol mixtures

E. Sloutskin,[1] O. Gang,[1,*] H. Kraack,[1] A. Doerr,[1,†] E. B. Sirota,[2] B. M. Ocko,[3] and M. Deutsch[1,‡]
[1]*Physics Department, Bar Ilan University, Ramat Gan 52900, Israel*
[2]*ExxonMobil Research and Engineering Company, Route 22 East, Annandale, New Jersey 08801, USA*
[3]*Physics Department, Brookhaven National Laboratory, Upton, New York 11973, USA*
(Received 16 October 2002; revised manuscript received 5 May 2003; published 23 September 2003)

Surface freezing is studied in dry and hydrated alcohol mixtures by surface x-ray scattering and surface tension measurements. A crystalline bilayer is formed at the surface a few degrees *above* the bulk freezing temperature. The packing is hexagonal, with molecules aligned along the surface normal in all cases. The in-plane lattice constant reveals a qualitatively different behavior with composition for hydrated and dry mixtures. The simple theoretical approach used successfully for alkane and deuterated alkane mixtures accounts well also for the alcohol mixtures. The repulsive length-mismatch term opposing the mixing entropy term in the free energy of the mixtures is shown to have a universal behavior for all mixtures studied: protonated alkanes, deuterated alkanes, and dry and wet alcohols. This universality is somewhat counterintuitive in view of the different interactions (e.g., hydrogen bonding in alcohols) in the different mixtures.

DOI: 10.1103/PhysRevE.68.031606 PACS number(s): 61.30.Hn, 68.35.Md, 68.03.Hj, 68.18.Jk

I. INTRODUCTION

The surface freezing (SF) effect in alkanes has been discussed in the preceding paper [1], denoted hereafter as I. The present paper deals with SF in melts of binary mixtures of alcohols. For melts of pure single-component samples, SF in alcohols differs from that in alkanes in several important aspects. In alkanes $[CH_3(CH_2)_{n-2}CH_3$, denoted by $C_n]$, the surface-frozen layer is a single molecule thick [2–4]. In alcohols $[CH_3(CH_2)_{n-2}CH_2OH$, denoted by $C_nOH]$, the SF layer is two molecules thick, i.e., it is a bilayer. The polar hydroxyl headgroups of both layers reside at the center of the bilayer, thus minimizing oleophobic-oleophilic interactions [5,6]. The range of chain lengths exhibiting SF in alkanes is $16 \leqslant n \leqslant 50$. In alcohols, however, only molecules with even number of carbons and chain length with $16 \leqslant n \leqslant 28$ undergo surface freezing. This odd-even effect is probably due to the different orientations of the terminal OH group relative to the molecular axis. This renders the formation of hydrogen bonds, which stabilize the two-layer structure of the SF film, unfavorable in odd alcohols [5,6]. The temperature range of existence, $\Delta T = T_s - T_f$, between the onsets of surface (T_s) and bulk (T_f) freezing in alcohols, $\lesssim 2\,^\circ$C, is smaller than that of alkanes, $\lesssim 3.5\,^\circ$C. The molecules in the SF layer are hexagonally packed, and are surface normal for $n < 24$. For $n > 24$, the molecules have a finite tilt θ in the next-nearest neighbor direction. Finally, while the surface-frozen phase in alcohols is a rotator phase with random molecular plane orientations for all $n \leqslant 26$, for $C_{28}OH$ the SF phase is fully crystalline, with herringbone order in the molecular plane orientations.

The existence of both van der Waals (vdW) interactions between the chains and hydrogen bonding (HB) between the hydroxyl groups in the SF alcohol bilayer allows fine tuning of the structure of the bilayers by bulk additives [5–8]. Thus, when water molecules are introduced into the system, they intercalate into the center of the bilayer and increase its thickness by a constant ~ 2.5 Å regardless of chain length n [5,6]. More importantly, the intercalated water molecules alter the hydrogen bonding, and impart an increased stability to the SF bilayer, reflected in higher T_s and T_f temperatures and larger existence ranges ΔT than those of the dry alcohols. The increased stability is due to an anomalously larger water solubility in the solid rotator phase as compared to the liquid phase. Thus, hydrated alcohols solidify at higher temperatures than the dry ones, both at the surface and in the bulk. However, the temperature shifts relative to the dry case are not equal for the bulk and the surface, rendering the existence ranges $\Delta T = T_s - T_f$ significantly larger than those in the dry samples [5,6]. The increased stability is also reflected in the considerable extension of the range of chain lengths for which SF occurs, from $16 \leqslant n \leqslant 28$ for the dry to $10 \leqslant n \leqslant 28$ for the hydrated alcohols. All the aspects of SF, other than those discussed above, are similar in alkanes and alcohols and are fully described in the Introduction of Paper I.

In this study we explore the SF effect in alcohol mixtures, both dry and hydrated, in order to elucidate the relative role and importance of vdW and HB interactions in the SF of alcohols, and to extract the ''universal'' characteristics of the effect, common to both alkanes and alcohols. From a theoretical point of view, the microscopic origins of SF in alcohols seem to be similar to those in alkanes [9–11], however the hydrogen bonding should produce a small but nonnegligible contribution [12]. As discussed for alkane mixtures, the use of alcohol *mixtures* provides an additional tuning knob for the chemical potentials, which can, and does [13,14], uncover new phases and phase transitions. For example, as demonstrated in a previous study [15], an alcohol which does not exhibit SF in its pure state, e.g., $C_{14}OH$, may undergo SF when mixed, even at a very low concentration,

*Present address: Physics Department, Brookhaven National Laboratory, Upton, NY 11973, USA.
†Present address: Continental AG, Jaedekamp 30, D-30419 Hannover, Germany.
‡Corresponding author. Email address: deutsch@mail.biu.ac.il

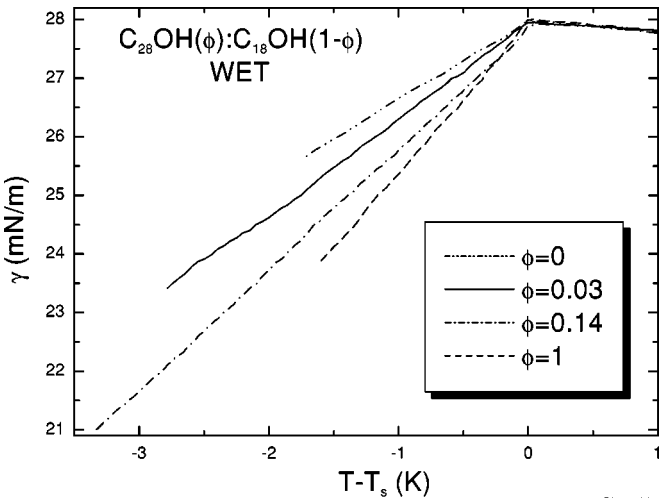

FIG. 1. Typical temperature T scans of the surface tension $\gamma(T)$ of hydrated $C_{18}OH+C_{28}OH$ mixtures, for the indicated $C_{28}OH$ concentrations ϕ. The curves end at the bulk freezing temperatures T_f. The cusp denotes the surface freezing temperature T_s. Small vertical shifts, all within the absolute experimental accuracy, were applied to the curves to make their $\gamma(T_s)$ coincide.

with another alcohol. The two-dimensional (2D) surface-frozen layer is a relatively simple system, and can be conveniently modeled theoretically using a mean-field thermodynamical approach based on the strictly regular mixture theory [16,17], as done for the alkane mixtures in Paper I. This provides a rare opportunity to investigate the very basic properties of the long-chain alcohol and alkane molecules, such as the intermolecular repulsion energy due to chain length mismatch, which are difficult to obtain from bulk measurements, due to the strong interlayer coupling and the significant kinetic barriers [15]. We find a practically identical behavior for the interchain repulsion energy in protonated-protonated alkane mixtures, deuterated-protonated alkane mixtures, both discussed in Paper I, and the dry and hydrated alcohol mixtures discussed in this paper. It is argued that this represents a universal behavior, common to SF of all alkyl-chain molecules.

The x-ray and surface tension measurements for a number of alcohol mixtures spanning a range of length differences are presented and discussed below. They are analyzed within the theoretical model presented in Paper I, modified to take into account the different structure of the SF layer and, for the hydrated samples, the presence of water in the mixture. This last point is discussed in detail in the Appendix. Finally, the universal features of the interchange energy are discussed for all mixtures studied in Paper I and the present paper.

II. EXPERIMENTAL TECHNIQUES

The surface phase boundaries were explored by surface tension (ST) measurements, using the Wilhelmy plate method (see Paper I). This also provides values for the entropy loss upon surface freezing. Several typical temperature scans of the ST of $C_{18}OH+C_{28}OH$ hydrated mixtures are shown in Fig. 1. Note the clear dependence of the sub-T_s slope on the bulk concentration ϕ. The way thermodynamical data are derived from the ST scans is the same as in Paper I. Note that considerable bulk undercoolings (generally of unknown magnitudes) exist in *mixtures* of alcohols [15]. Thus, the bulk freezing temperatures obtained in ST measurements on dry alcohol mixtures do not correspond in many cases to the thermodynamical equilibrium freezing temperatures. Thus, we did not attempt to address the bulk liquid-solid transition of the dry alcohol mixtures in this paper. For hydrated alcohols, the supercooling problems are much less severe, as shown in an earlier study [15], and their freezing temperatures are included in this study.

The structure of the SF bilayer was explored by surface-specific synchrotron x-ray measurements. The surface-normal electron density profiles were obtained from x-ray reflectivity (XR) measurements as a function of the surface-normal momentum transfer q_z. The in-plane 2D lattice structure and molecular tilt directions and magnitudes were measured by grazing-incidence diffraction (GID) measurements as a function of the surface-parallel momentum transfer q_r, and Bragg-rod (BR) measurements along q_z at the positions of the GID peaks. The x-ray measurements were carried out using synchrotron radiation at beam line X22B, NSLS. The pure components were obtained from Sigma-Aldrich-Fluka, and were labled at least $\geqslant$97% pure. The mixtures were prepared by weighing the required amounts for a total volume of 0.3 cm^3 (ST) or 0.7 cm^3 (x rays), heating them to at least 10 °C above the melting point of the higher-molecular weight component, and stirring vigorously on a hotplate with a magnetic stirrer for >15 min. For the experiments on hydrated alcohols, a ring-shaped water trough with 2–3 cm^3 of water surrounded the alcohol container which resided inside the sample cell. This generated a saturated water vapor atmosphere in the cell. The sample was hydrated by absorbing water from the vapor. A complete restitution of all the properties measured on the dry sample was observed upon drying of the hydrated samples.

The measured XRs of the surface crystalline phase were analyzed quantitatively using a layered interface (''box'') model. The box model, used also in previous mixture studies [5,6,15] and in Paper I, consists of four slabs: (1) the $(CH_2)_{n-1}$ chain of the upper layer, (2) the OH head groups region, (3) the $(CH_2)_{n-1}$ chain of the lower layer [same as box (1)], and (4) the CH_3 terminal group at the bilayer-liquid bulk interface. An additional box represents the liquid subphase. Three different roughness parameters were assumed: (1) at the bilayer-vapor interface, (2) the upper and lower interfaces of the OH slab, and (3) at the bilayer-liquid bulk interface. The model used for fitting the BR is the same used for pure alcohols [6].

Further details of the experimental setup and techniques used are given in Paper I and in Refs. [6,15,18].

III. RESULTS: THERMODYNAMICS

In this section we present results extracted from the surface tension measurements on the various binary alcohol mixtures studied, and their analysis by the theoretical model

presented below. The measured quantities for the various mixtures are listed in Table I.

A. The phase behavior

1. Experimental results

The surface freezing temperatures T_s of the dry alcohol mixtures, measured by ST, are plotted in Fig. 2 (points), vs the liquid bulk concentration $\phi = N/(N+M)$, where N is the number of the long-chain molecules and M is the number of the short-chain molecules in the liquid bulk. Note the almost linear $T_s(\phi)$ for $C_{18}OH + C_{22}OH$ and for $C_{14}OH + C_{18}OH$. Upon increasing the relative chain mismatch between the pure components, $\Delta n/\overline{n} = 2(n-m)/(n+m)$, where n,m are the carbon numbers of the two components, a more curved $T_s(\phi)$ is observed. For very large $\Delta n/\overline{n}$ (e.g., $C_{18}OH + C_{26}$ OH) the mixture reverts to a solutionlike behavior, where $T_s(\phi)$ is linear in $\ln\phi$ for $\phi \gtrsim 0.2$ and linear in $\ln(1-\phi)$ for $\phi \lesssim 0.2$ [18,19]. In our case, no SF is observed for nearly equimolar mixtures with high interchain mismatch. Such regions, e.g., the dashed line region for $C_{18}OH + C_{28}OH$ mixtures in Fig. 2, where no SF occurs, were nicknamed ''black holes'' in Paper I. Black holes were also observed in Paper I in similarly large-$\Delta n/\overline{n}$ alkane mixtures. An intriguing new effect is exhibited by the $T_s(\phi)$ curve of $C_{18}OH + C_{24}OH$: the surface freezing point of the mixture at $\phi \approx 0.1$ is lower by 1–2 °C than the T_s of either of the pure components of the mixture. It is widely known that the *bulk* freezing point of a material can often be lowered by mixing with a second, even higher-freezing-point, material. However, no similar effect was observed to date for the *surface*-frozen phases.

The behavior of the hydrated alcohol mixtures, shown in Fig. 3 (points) is very similar to that of the dry mixtures, except for the hydrated $T_s(\phi)$ being usually shifted up from the corresponding dry $T_s(\phi)$ by a few degrees. As discussed in the Appendix, using $\phi = N/(N+M)$ for the concentration of the hydrated mixture instead of the rigorous $\phi_{real} = N/(N+M+W)$, where W is the number of water molecules in the system, is, to a good approximation, the same as assuming that the hydration level is linear in $N/(N+M)$. The agreement of the measured values with the theory, discussed below, supports the validity of this approximation for all hydrated mixtures addressed here. As for the dry mixtures, an almost linear $T_s(\phi)$ is found for a small relative chain length mismatch $\Delta n/\overline{n}$, while significant deviations from linearity are exhibited by mixtures with large $\Delta n/\overline{n}$. The hydration reduces the tendency to form black holes in large-$\Delta n/\overline{n}$ mixtures, as reflected, for example, by the smaller ϕ range of the black hole in the hydrated $C_{18}OH + C_{28}OH$ mixture in Fig. 3 as compared to the dry one in Fig. 2. This reduction in the ϕ range is a result of the anomalously larger water solubility in the surface-frozen rotator phase as compared to that in the liquid surface phase [6,5]. This causes larger upshifts in T_s than in T_f, thus increasing ΔT and decreasing the ϕ-range where SF is preempted by bulk freezing, i.e., the ϕ range of the black hole. As Fig. 3 shows, hydration also induces SF in the pure, $\phi = 0$, $C_{14}OH$ whereas no SF occurs in the dry sample (Fig. 2). All of these effects indicate an increased stability for the SF phase in hydrated alcohol mixtures as compared to the dry ones. This conclusion is in agreement with that drawn from measurements on pure alcohols [6,5].

The *bulk* freezing temperatures $T_f(\phi)$ of $C_{18}OH + C_{22}OH$ and $C_{18}OH + C_{28}OH$ mixtures, as obtained in ST measurements, are also shown in Fig. 3 (half-solid symbols). A prominent minimum is observed at $\phi \approx 0.1$ for $C_{18}OH + C_{28}OH$. This minimum is a feature common to most mixtures investigated, and is characteristic of a solutionlike behavior. However, the *measured* $T_f(\phi)$ points do not exhibit at $0.1 \lesssim \phi \lesssim 0.2$ the sharp slope change expected for ideal solutions [19,18], but rather indicate a rounded, continuous slope change, observed in the measured points for both $C_{18}OH + C_{22}OH$ and $C_{18}OH + C_{28}OH$ in Fig. 3. The bulk phase diagram of hydrated mixtures with a small-chain length mismatch $\Delta/\overline{n}$ do not exhibit significant T_f hysteresis. However, for the $C_{18}OH + C_{28}OH$ compound, it is highly probable that supercooling occurs over a significant ϕ range, particularly in the vicinity of black holes, an effect found in other samples [18–20].

2. Theoretical analysis

The same theoretical model employed for the alkane and deuterated alkane mixtures in Paper I was also used here for the dry and the wet alcohol mixtures. The liquid phase was assumed to be an ideal mixture, while for the solid phase the strictly regular mixture theory was adopted [16,17]. This introduced an additional term in the free energy, accounting for the chain length mismatch $\Delta n/\overline{n}$. This mean-field-like term is proportional to the average number of pair interactions between long and short molecules and to the interchange energy $\omega_{b,s}$ (here ω_b is used for the interaction energy in the bulk, and ω_s—at the surface) [16,17]. The long molecules occur in the solid with a probability $N^s/(N^s+M^s)$, where N^s (M^s) is the number of long (short) species *in the solid phase*. The short molecules occur with a probability $M^s/(N^s+M^s)$. The arguments justifying the use of these expressions, and the theory of Paper I, which are valid for binary mixtures, for the hydrated mixtures, which should properly be treated as ternary mixtures, are given in the Appendix. Note also that the theory used for the alkanes in Paper I assumed a linear variation with ϕ of the contribution of the internal degrees of freedom to the system's free energy, a reasonable assumption for chains interacting only via a vdW potential. The validity of this theory for alcohols, which have a polar headgroup and interact by both vdW and HB potentials, is not self-evident. Its application to alcohols assumes implicitly that the energetic contribution of the HB-interacting OH groups to the free energy also varies linearly between the values of the pure components, i.e., those at $\phi = 0$ and at $\phi = 1$. Several good reasons can be given why such an assumption should not be valid. However, the good fits of the theoretical expressions to the experimental data with only a single fit parameter $\omega_{b,s}$ as well as the universality of the behavior of $\omega_{b,s}$ for all mixtures, includ-

TABLE I. Thermodynamical and structural results for the SF layer of binary alcohol mixtures. ϕ is the mole fraction of the longer component. The surface tension measured thermodynamical quantities are the surface (T_s) and the bulk (T_f) freezing temperatures, and the entropy loss per unit area upon SF (ΔS). The structural quantities measured by XR and GID are the half thickness of the surface frozen bilayer d and the lattice spacing a. The "black-hole" regions, where SF does not occur, are marked by "–." For the wet $C_{18}OH + C_{28}OH$, $\phi = 0.2$ mixture two different values are given for the bilayer half thickness d, one below and one above the demixing transition.

ϕ	T_f (°C)	T_s (°C)	ΔS (mJ/[m^2 K])	d (Å)	a (Å)
			$C_{18}OH + C_{22}OH$ Dry		
1	69.7	70.55	2.19	29.4	4.854
0.82	66.4	67.8	1.97		
0.77				28.9	4.840
0.66	63.5	65.4	2.08	28.7	
0.45	59.0	61.8	2.28	27.6	4.837
0.26	56.35	59.3	2.04	26.0	4.836
0.17	55.4	58.5	2.10		
0.1	55.5	58.25	2.02	24.9	4.842
0.07	56.0	58.1	2.04		
0	57.6	58.2	2.04	24.8	4.820
			$C_{18}OH + C_{22}OH$ Wet		
1	72.3	74.0	1.84	30.56	4.942
0.82	69.35	71.35	1.74		
0.77				30.2	
0.66	67.3	69.5	1.90		
0.45	63.25	65.85	2.12	28.7	4.853
0.26	60.6	63.4	1.83	27.2	4.857
0.17	59.35	62.3	1.96		
0.1	59.45	62.25	1.90	26.1	4.859
0.07	59.2	61.6	1.88		
0	60.0	61.77	1.90	25.6	4.946
			$C_{18}OH + C_{26}OH$ Dry		
1	77.96	78.66	2.77	33.2	4.902
0.86	75.4	76.3	2.22		
0.73	73.4	74.4	1.07	32.8	–
0.62	72.7	72.7	–	–	–
0.51	69.5	69.5	–	–	–
0.41	67.0	67.0	–	–	–
0.32	65.0	65.0	–	–	–
0.23	57.6	59.0	3.98	33.5	4.769
0.2				31.3	
0.19				31.5	4.784
0.15	54.0	57.0	2.01	24.6	4.868
0.11	54.15	57.35	2.03		
0.07	55.1	57.5	1.94		
0.04	56.0	57.7	1.82		
0	57.2	57.7	2.1	24.8	4.82
			$C_{18}OH + C_{26}OH$ Wet		
1	80.65	82.0	2.86		
0.86	78.2	79.3	3.10		
0.73	75.55	77.35	2.86	35.0	4.846
0.62	73.2	75.2	3.53		
0.51	70.3	72.5	3.28		
0.41	67.2	70.2	3.25	34.2	4.819
0.32	63.5	67.5	2.97		
0.23	60.7	62.7	3.07		
0.19				28.2	4.843
0.15	58.65	61.75	2.08	26.5	4.857
0.11	57.6	61.4	2.02		
0.07	58.2	61.5	1.95		
0.04	59.2	61.8	1.91		
0	60.0	61.75	1.96	25.6	4.946

TABLE I. (*Continued*).

ϕ	T_f (°C)	T_s (°C)	ΔS (mJ/[m^2 K])	d (Å)	a (Å)
			$C_{16}OH+C_{22}OH$ Dry		
1	70.0	70.65	1.97	29.4	4.854
0.87	67.3	67.95	2.46	29.5	4.839
0.74	65.2	65.55	2.78	29.3	4.824
0.63	62.48	–	–	–	–
0.52	59.3	–	–	–	–
0.42	56.0	–	–	–	–
0.34	53.0	–	–	–	–
0.31	49.7	52.6	2.26		
0.28	48.25	51.4	2.40	26.4	4.828
0.2	46.6	49.6	1.81		
0.15	45.7	49.3	1.79	23.3	4.831
0.11	45.5	49.2	1.78		
0.07	46.4	49.1	1.65		
0.04	47.5	49.2	1.45		
0	48.9	49.25	1.36		
			$C_{16}OH+C_{22}OH$ Wet		
1	72.8	74.6	1.92	30.6	4.942
0.87	70.0	71.8	2.05	30.8	4.855
0.74	67.3	69.1	2.39	30.7	4.838
0.63	64.6	66.6	2.45	30.6	4.846
0.52	61.55	64.04	2.60	29.2	4.847
0.42	57.2	59.7	2.23		
0.34	54.1	57.0	2.24		
0.31	53.7	56.6	2.15		
0.28	51.9	54.7	2.21	27.5	4.837
0.2	50.9	53.9	1.74		
0.15	49.9	53.4	1.60	24.9	4.849
0.11	49.6	53.35	1.58		
0.07	49.8	53.4	1.48		
0.04	50.9	53.7	1.47		
0	51.9	53.8	1.47	23.0	4.891
			$C_{18}OH+C_{28}OH$ Dry		
1	81.8	82.9	2.32	35.1	
0.92	80.9	81.85	2.72		
0.85	80.1	80.5	2.83		
0.78	78.5	79.4	2.93		
0.72	79.0			35.3	
0.6	77.5	–	–	–	–
0.49	75.0	–	–	–	–
0.39	70.5	–	–	–	–
0.3	67.4	–	–	–	–
0.22	64.0	–	–	–	–
0.14	57.1	–	–	–	–
0.1	54.3	57.3	2.13	–	–
0.07	55.24	57.54	1.88	24.4	
0.03	56.25	57.9	1.83		
0	57.5	58.0	1.88	24.8	

TABLE I. (*Continued*).

ϕ	T_f (°C)	T_s (°C)	ΔS (mJ/[m^2 K])	d (Å)	a (Å)
			$C_{18}OH+C_{28}OH$ Wet		
1	84.25	85.8	2.77	37.8	4.956
0.92	83.3	84.7	2.80		
0.85	82.0	83.4	2.83		
0.78	80.8	82.0	3.38		
0.72	79.0	80.9	3.72	38.2	4.859
0.6	76.5	78.2	3.38		
0.49	73.8	75.5	3.25		
0.39	68.0	–	–	–	–
0.3	65.8	68.0	3.18		
0.22	63.0	64.8	3.63	38.5	4.770
0.2				33.3,38.6	
0.14	58.0	61.37	2.12		
0.1	57.5	61.5	2.04		
0.07	57.8	61.28	2.00		
0.03	58.8	61.6	1.80		
0	60.15	61.8	1.77	25.6	4.946
			$C_{18}OH+C_{24}OH$ Dry		
1	74.8	75.4	2.55	31.4	4.878
0.87	72.55	73.25	2.55	31.1	
0.69	67.35	69.15	2.20	31.7	
0.53				31.2	
0.49	62.8	64.9	2.55		
0.33	58.6	61.6	1.90	30.1	4.870
0.25	55.8	58.6	1.90		
0.16	54.8	57.0	1.40	30.1	
0.1	54.1	56.45	1.90		
0.06	54.7	56.25	1.70		
0	57.45	58.15	1.70	24.8	

ing alcohols, as discussed below, strongly supports the validity of our theoretical model also for alcohols.

The theory in Paper I requires values of various thermodynamical quantities of the pure components. As pointed out in Paper I, the ST measurements yield the entropy loss upon SF per unit area. Since the area/molecule in the liquid surface phase is not known, we used the measured [21] dry bulk entropy loss per molecule in the calculations of both the dry and the wet alcohols, bulk and surface. For the absolute surface tension of pure alcohols (γ_n, γ_m) we used a second-order polynomial extrapolation of published values [22], which, unfortunately, extend to only $n \leqslant 18$. Because of unavoidable variations in cutting the paper plates to size, and their depth of immersion in the sample melt, the absolute values of the surface tension can be trusted only to ~ 1 mN/m. To within this somewhat limited *absolute* accuracy, our *relative*-scale [1] ST measurements agree with the extrapolated values for both dry and hydrated alcohols. No consistent shifts in the ST values between dry and hydrated samples were detected. In any case, since only ($\gamma_n - \gamma_m$) is used in the equations, consistent shifts of nearly equal size would cancel out. Finally, we remind the reader that ω_s is varied in the fit until the best agreement between the measured and calculated $T_s(\phi)$ is achieved. For further details, and the equations used, see Paper I.

The theoretical fits to the measured $T_s(\phi)$ are shown in solid lines in Fig. 2 for the dry alcohol mixtures and in Fig. 3 for the wet ones. In a black-hole region, the theoretical fit is plotted with a dashed line. However, the ϕ boundaries of this region are not calculable accurately from theory. The values of ω_s extracted from the fit are discussed below.

In the dry mixtures, the bulk behavior is complicated by kinetic effects (e.g., supercooling), making the phase boundary difficult to obtain experimentally and to describe theoretically. By contrast, the hydrated small-$\Delta n/\overline{n}$ mixtures do not show significant bulk supercoolings. However, for large-$\Delta n/\overline{n}$ mixtures supercooling should become significant even for hydrated alcohols [18]. Indeed, the formulas used for bulk alkane mixtures in Paper I provide excellent fits for the small-$\Delta n/\overline{n}$ hydrated alcohol mixtures, as can be observed for the $C_{18}OH+C_{22}OH$ mixtures in Fig. 3. However, at larger $\Delta n/\overline{n}$ deviations of the theory from the experiment become significant, as can be seen for the $C_{18}OH+C_{28}OH$ bulk freezing temperatures $T_f(\phi)$ in Fig. 3 (dash-dot line and semiclosed circles). The points in the vicinity of a black hole are generally expected to supercool more than ϕ regions where SF exists. This is because the SF layer provides additional nucleation sites for the bulk solid, reducing the kinetic barrier for nucleation, and hence also reducing the supercooling T range. For the bulk mixture of $C_{18}OH+C_{28}OH$, shown

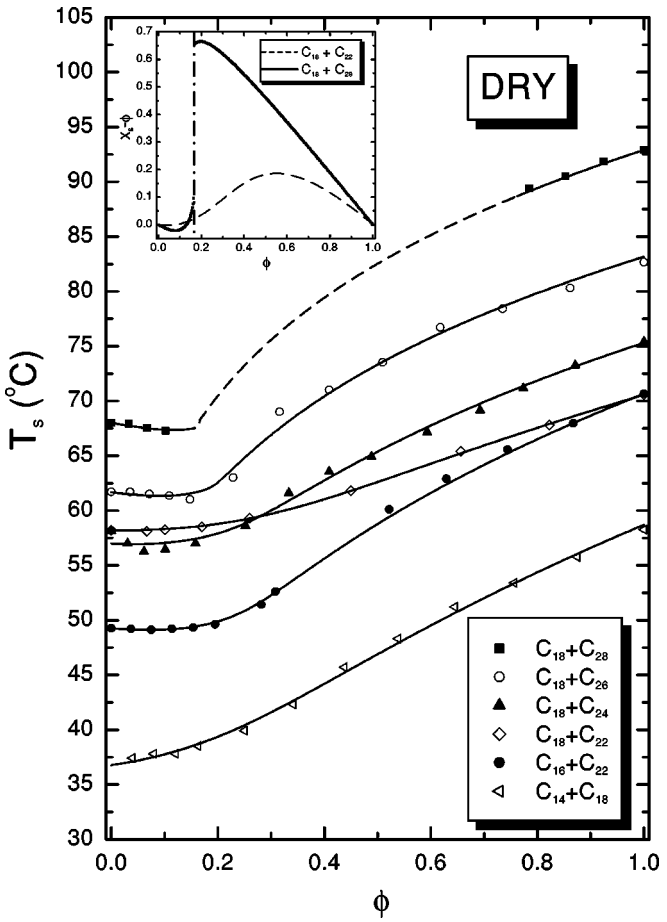

FIG. 2. Surface freezing onset temperatures T_s of dry alcohol mixtures. ϕ is the mole fraction of the longer component in the liquid phase. The experimental data are shown by points. The lines were obtained by fitting the theoretical expression for $T_s(\phi)$ to the measured values refining the interchange energy of the components, as described in the text. The dashed line for $C_{18}OH+C_{28}OH$ denotes a "black-hole" region where surface freezing does not occur. The $C_{18}OH+C_{26}OH$ and the $C_{18}OH+C_{28}OH$ mixtures were upshifted for clarity by 4 and 10 °C, respectively. The excess molar concentration of the long component in the surface-frozen phase, x_s over the bulk liquid phase concentration ϕ, is shown in the inset for $C_{18}OH+C_{22}OH$ (dashed line) and $C_{18}OH+C_{28}OH$ (solid line) mixtures. Note the discontinuity at $\phi\approx 0.2$ for $C_{18}OH+C_{28}OH$ (dash-dotted vertical line) and the negative values below this singularity. No similar features are observed for $C_{18}OH+C_{22}OH$, where only small deviations of x_s from ϕ are observed. The $(x_s-\phi)$ curves shown in the inset are obtained from the theory, as described in the text; note that these curves are meaningful only outside the black holes.

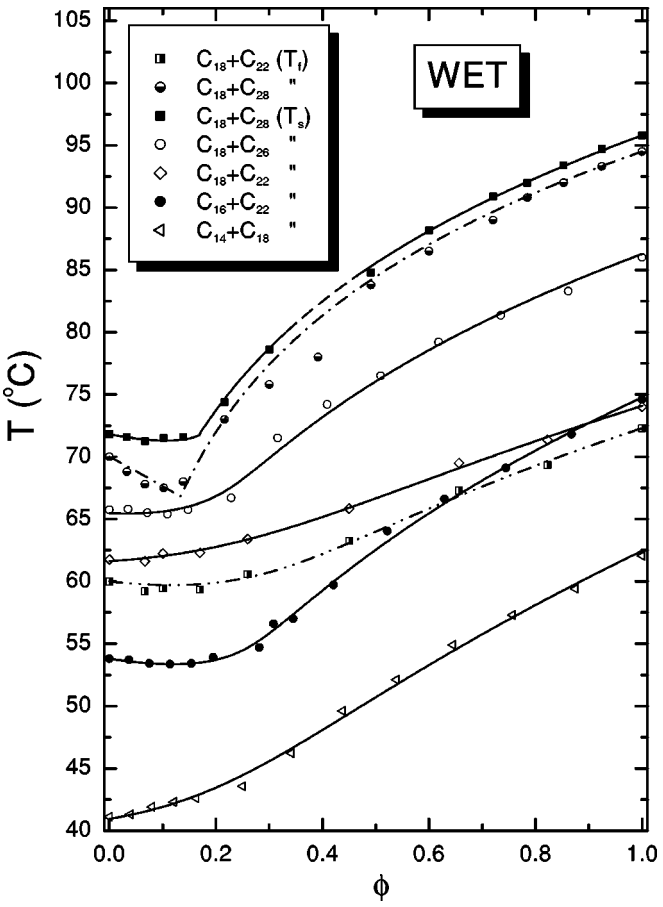

FIG. 3. Same as Fig. 1, but for hydrated mixtures. The measured *bulk* freezing temperatures T_f are also shown for $C_{18}OH+C_{22}OH$ (semisolid squares) and $C_{18}OH+C_{28}OH$ (semisolid circles) along with the theoretical fits (dash-dotted lines). The black-hole region of $C_{18}OH+C_{28}OH$ is shown by a dashed line. The $C_{18}OH+C_{26}OH$ and $C_{18}OH+C_{28}OH$ data were upshifted for clarity by 4 and 10 °C, respectively.

in Fig. 3, two experimental points at $\phi=0.3$ and 0.39 adjacent to the black-hole region, $0.35\lesssim\phi\lesssim 0.48$, are indeed found to lie well below the theoretical curve, indicating the existence of a considerable nucleation barrier and of supercooling.

The fits of the theoretical model to the measured $T_s(\phi)$ values yield, in addition to ω_s, also the concentration $x_s(\phi)$ of the longer component in the *solid* surface phase. As discussed in Paper I, x_s differs from the bulk nominal ϕ due to the Gibbs-like enrichment of the surface by the lower-surface-energy component. In our mixtures this is the longer component for almost all alcohols and ϕ. The surface enrichment of the solid phase, $x_s-\phi$, is shown in the inset to Fig. 2 for two typical cases representing mixtures with small and large length mismatch. The small-$\Delta n/\bar{n}$ mixtures, represented by the $C_{18}OH+C_{22}OH$ shown by a dashed line, form an almost ideal mixture in the surface-frozen phase. In this case x_s exceeds ϕ only slightly, peaks at nearly equimolar ϕ, and the deviation is continuous in ϕ. For large-$\Delta n/\bar{n}$ mixtures, represented by $C_{18}OH+C_{28}OH$ shown in a solid line, the deviations $x_s-\phi$ are much larger, with peaks shifted to lower ϕ. For very large $\Delta n/\bar{n}$ a discontinuity occurs in x_s, as shown by the dash-dot line in the inset. For this mixture the deviation of x_s from the bulk concentration ϕ reaches $\sim 300\%$ and peaks at $\phi=0.2$. Since the x_s discontinuity at $\phi=0.2$ is located within a black hole, where SF does not occur, no demixing effect on the SF phase can be observed. However, for the same hydrated mixture, where the black-hole is much smaller, SF does exist at $\phi=0.2$. As discussed below and elsewhere [13], a discontinuous demixing transi-

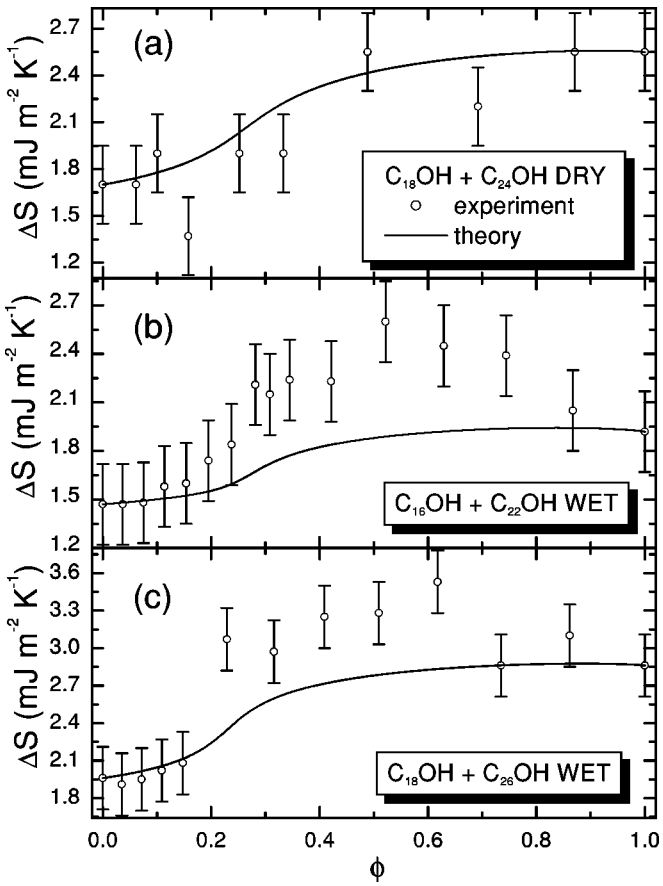

FIG. 4. The measured (points) surface entropy loss upon surface freezing, ΔS, for one dry and two hydrated alcohol mixtures. The theoretical predictions, having no adjustable parameters, are shown by solid lines. Note the maxima appearing in the experimental data at $\phi \approx 0.5$ for high-$\Delta n/\bar{n}$ mixtures [(b) and (c)], which our simple theory cannot reproduce. For discussion see text.

tion occurs here in the SF bilayer, resulting in the observation of a solid-solid thin-thick transition in the bilayer.

B. Entropy

The entropy loss upon SF, $\Delta S(\phi)$, is an important thermodynamical quantity, obtainable from the slope change of the $\gamma(T)$ curve upon SF (see Paper I). Figure 4 shows the measured $\Delta S(\phi)$ (points) for several dry and hydrated mixtures. Since the entropy of pure molten alcohols grows roughly linearly with the molecular length n in the length range addressed here, their entropy loss upon SF also grows with the molecular length n [3,2]. In mixtures, the entropy loss upon SF is also influenced by changes in the mixing entropy [15], which, in turn, depends on the different compositions of the liquid (ϕ) and solid (x_s) phases. Therefore, it is not surprising that a nonlinear $\Delta S(\phi)$ is measured, as shown in Fig. 4(a). Moreover, the measured $\Delta S(\phi)$ shown in Figs. 4(b,c) exhibit a small, broad maximum at $\phi \approx 0.5$. This peak in the entropy loss may result from ϕ-dependent restrictions on the complete randomality of the packing of the molecules in the solid phase. If these restrictions become most prominent near equimolar mixtures, the solid phase entropy will be reduced most for these mixtures, causing the observed maximum in $\Delta S(\phi)$. Another likely reason for the maximum in $\Delta S(\phi)$ is the anomalously high heat capacity of the rotator phase (known to occur in the bulk) which results in curvature in $T_f(\ln \phi)$ as ϕ decreases from unity, as discussed in the Appendix of Ref. [19].

Using the $x_s(\phi)$ values obtained from the theoretical fits to the measured $T_s(\phi)$ values, and without any adjustable parameters, we calculate the theoretical entropy losses upon SF, $\Delta S(\phi)$, and compare them (lines) with the measured values (points) in Fig. 4. The expression used for calculating $\Delta S(\phi)$ is identical with Eq. (14) in Paper I, multiplying the result by a factor of 2 due to the bilayer structure of the SF phase. For $n \geqslant 22$ the pure alcohol SF phase comprises tilted molecules, while for alcohol mixtures no tilted phases are found. The possible entropy change due to the loss of tilt upon mixing with $n < 22$ molecules was neglected in the calculation. The theoretical lines in Fig. 4 agree well with the measured values for small $\Delta n/\bar{n}$, as demonstrated in Fig. 4(a) for $C_{18}OH + C_{24}OH$, and in a previous study of $C_{14}OH + C_{18}OH$ [15]. However, for large $\Delta n/\bar{n}$ the shallow peaks at $\phi \approx 0.5$ can not be described well within our simplistic theoretical model, and deviations are observed in Figs. 4(b,c) in this ϕ region. We remind the reader, however, that the results shown in Fig. 4 are not fits but theoretical predictions without adjustable parameters. They are based on the results of fits to $T_s(\phi)$, where only a single unknown parameter ω_s is refined. Even this parameter is shown to have a universal behavior for all the chain molecule mixtures studied, including alcohols and alkanes. With this in mind the theory-experiment agreement for $\Delta S(\phi)$ can be deemed reasonably good.

IV. RESULTS: STRUCTURE

The values obtained in the x-ray measurements for both the surface-normal and surface-parallel structure of the surface-frozen bilayer are listed in Table I. We now discuss the x-ray results in detail.

A. X-ray reflectivity

A representative set of x-ray reflectivities measured for the SF phases of dry $C_{16}OH + C_{22}OH$ mixtures, is shown in Fig. 5. As can be readily seen, the ideal Fresnel reflectivity, $R_F(q_z) \sim q_z^4$, is strongly modulated by the finite thickness, high-density SF bilayer residing at the liquid-vapor interface of the mixtures. The layer thickness, $d_{bilayer} \approx 2\pi/\Delta q_z$, is inversely proportional to the period Δq_z of these Kiessig-like fringes. The period increases as $\phi \rightarrow 0$, indicating a decreasing thickness for the SF bilayer. This is as expected, since the fraction of short molecules in the SF bilayer should increase with that of the bulk when $\phi \rightarrow 0$. A quantitative analysis was done by fitting the measured XR (points) by the four-slab model discussed above. The fits are shown by lines in Fig. 5. The corresponding surface-normal electron density profiles derived from the fit are plotted in the inset. The only consistent variation observed in the density profiles as ϕ is

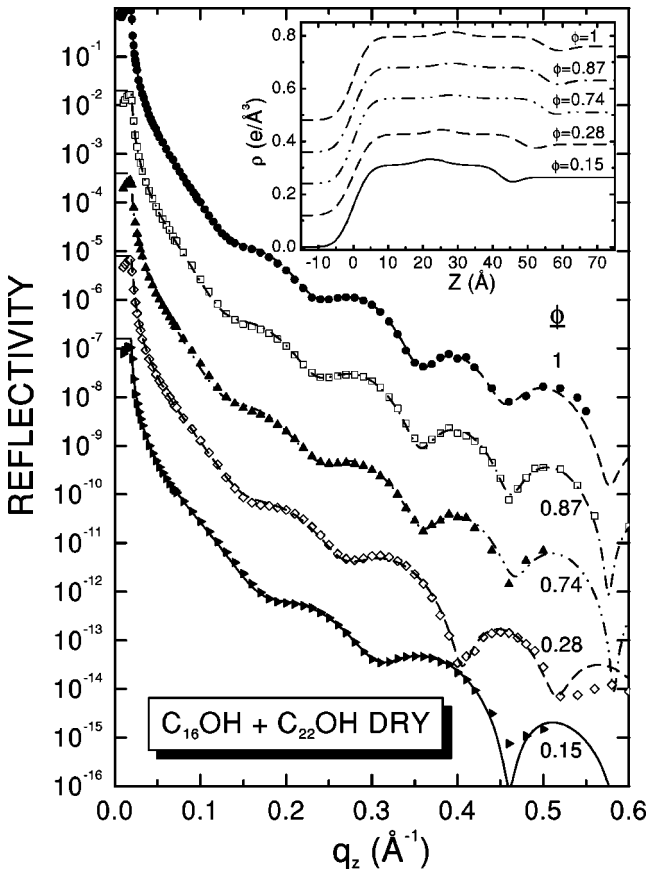

FIG. 5. X-ray reflectivities (points) for the surface-frozen phase of $C_{16}OH+C_{22}OH$ Dry mixtures. The fringe period is inversely proportional to the bilayer thickness, which is seen to grow monotonically with the concentration of $C_{22}OH$ in the mixture, ϕ. The lines are fits by a four-slab model, and the corresponding surface-normal electron density profiles are shown in the inset. The reflectivities and the density profiles are shifted vertically, for clarity.

varied, is a systematic reduction in the SF layer's thickness as $\phi \rightarrow 0$, as shown in Fig. 6(a) (open circles) for these mixtures.

B. Layer thickness

The half-bilayer thickness $d(\phi)=d_{bilayer}/2$ refined in the XR fits for several representative mixtures is plotted in Fig. 6. While the $C_{18}OH+C_{22}H$ data [(b), open circles for dry mixtures, solid squares for the wet mixtures] interpolates almost linearly between the d values of the SF layers of the pure materials, mixtures with larger $\Delta n/\bar{n}$ show a significantly more curved ϕ dependence, and even a discontinuous behavior, as for $C_{18}OH+C_{28}OH$ in Fig. 6(c). This trend, analyzed quantitatively below, is easy to understand qualitatively: as the chain length mismatch grows, the energy cost for close packing chains of unequal lengths, and the corresponding term in the free energy, also grow. The mixing entropy term, which has the opposite sign, is much less affected by the length variation, and thus the free energy increases upon increasing chain length mismatch. The mixture attempts, therefore, to reduce its energy by lowering the number of short molecule–long molecule contacts, i.e., by driving out one of the components. Hence the increasing deviations of x_s from ϕ (as shown, e.g., in the inset to Fig. 2) and the consequent deviations of $d(\phi)$ from a linear variation with ϕ, observed in Fig. 6 upon increasing the molecular length mismatch.

For a very large length mismatch, discontinuous behavior is observed in d, as can be seen in Fig. 6(c) at $\phi=\phi_{tr} \approx 0.2$. Such a transition was studied in a hydrated $C_{18}OH+C_{28}OH$ mixture [13], where a temperature-induced thin-thick solid-solid quasi-2D phase transition was found at ϕ values close to ϕ_{tr}. Accordingly, in Fig. 6(c) two points are shown for the *same* sample of a wet $\phi=0.2$ mixture. At a temperature $T \approx 64\,^{\circ}\mathrm{C}$ a thin layer, $d \approx 33.5$ Å, is observed with a $C_{28}OH$ concentration $x_s=0.3$. As the temperature is decreased to below $T \approx 63.4\,^{\circ}\mathrm{C}$ a new free energy balance is achieved, and a solid-solid transition occurs in the SF bilayer, to a higher $C_{28}OH$ concentration, $x_s=0.7$, and a correspondingly higher $d \approx 38.5$ Å.

The $x_s(\phi)$ values derived from the $T_s(\phi)$ fits can be used to calculate, independently from the values refined from the XR measurements, the surface-frozen bilayer's half thicknesses d using the known d values [6] of the pure components. The simplest approach is a linear interpolation:

$$d(\phi)=(x_s d_n/\cos\theta_n+[1-x_s]d_m)\cos(\theta_n x_s), \qquad (1)$$

where $x_s=x_s(\phi)$, θ_n is the tilt angle of the pure long component (the short pure components addressed here are always untilted), and d_n and d_m are the pure components' bilayer half thicknesses [6]. The increase in the bilayer thickness upon hydration by ~ 2.5 Å, due to the water molecules' intercalation into the bilayer's center [5,6] is taken into account by using the hydrated pure component values for d_n and d_m. Note that we have assumed that the effective contribution to the thickness from the tilt is linear in the concentration of the long component, i.e., $\cos[\theta(\phi)]=\cos(\theta_n x_s)$, so that $\theta(\phi)$ varies from $\theta=0$ to $\theta=\theta_n$. This approach is an oversimplification of the real behavior, since our BR scans show that the molecules are already untilted at a very low concentration of the untilted component ($x_s \rightarrow 1$). Moreover, the change from tilted to untilted molecules is restricted to a very small x_s region and may even be discontinuous with x_s. However, a comparison of the d value of the pure *tilted* long components [$\phi=1$, in Figs. 6(c) and 6(d)] with those of the mixtures, particularly at $\phi \lesssim 1$, indicates that within our accuracy, the effect of the change in the tilt is small. Thus, the linear approximation $\theta(\phi)=\theta_n x_s$ can be considered as a reasonable first approximation, which considerably simplifies the $d(\phi)$ calculations. The $d(\phi)$ curve calculated using Eq. (1) is shown by solid (dry mixtures) and dash-dot (hydrated mixtures) lines in Fig. 6. Considering that this curve has no adjustable parameters, the agreement is good for all mixtures shown. However, the best agreement is obtained for small $\Delta n/\bar{n}$, as demonstrated by the $C_{18}OH+C_{22}OH$ mixture in Fig. 6(b), and our previous study of $C_{14}OH+C_{18}OH$ [15].

The poorer agreement between the measured and calculated d for large-$\Delta n/\bar{n}$ mixtures indicates the need for a more sophisticated expression. As a next-order approximation a

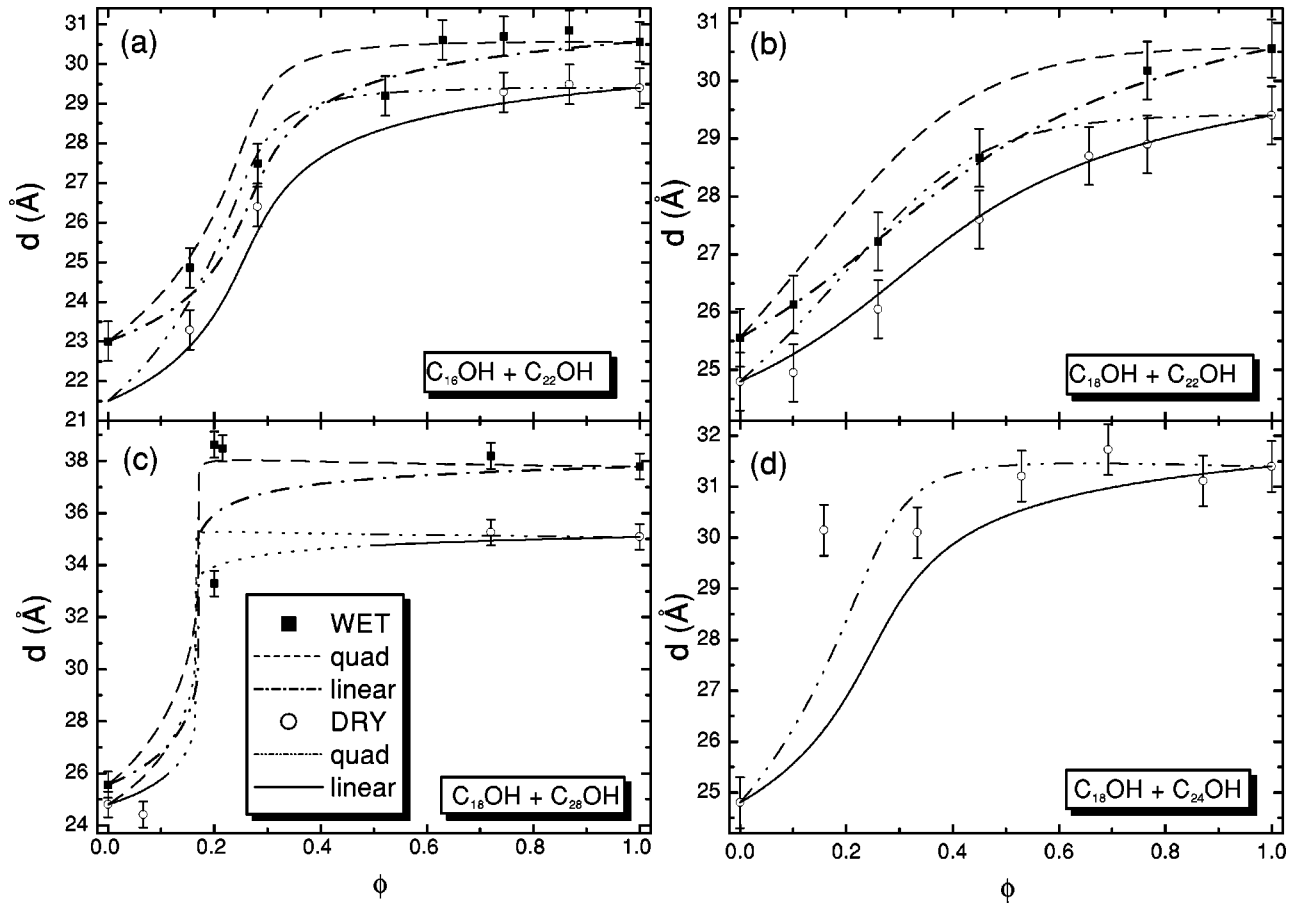

FIG. 6. The half thickness $d(\phi)$ of the surface-frozen bilayer of several dry (open circles) and hydrated (solid squares) alcohol mixtures, as obtained from the fits to the reflectivity measurements. To compare the thickness data, obtained experimentally, with the theoretical predictions one may use either the linear (solid line for dry, dash-dotted line for wet) or the quadratic (dash-dot-dot for dry, dash for wet) interpolations discussed in the text. Note that while the linear interpolation yields better results at the low-$\Delta n/\bar{n}$ limit (b), the quadratic one works better for high $\Delta n/\bar{n}$ (c) and (d). The dotted region in (c) marks a black-hole region.

second-order polynomial was employed, and found to describe better the behavior of d [13]:

$$d(\phi)=\{d_n[x_s^2+2x_s(1-x_s)]/\cos\theta_n+d_m[1-x_s]^2\}\times\cos(\theta_n x_s). \quad (2)$$

Here, the assumption is that the contributions to the x-ray reflectivity are taken in pairs of adjacent molecules, and that the contribution of a pair consisting of a long and a short molecule is the same as that of a long-long pair. The (equal) contributions of these two combinations are taken to be different from that of a short-short pair. Using this specific weighting-by-pairs scheme to interpolate the layer's half thickness $d(\phi)$ between those of the pure components, yields the quadratic expression of Eq. (2) above. Since no direct measurement of x_s can be made with our setup, we cannot verify Eq. (2) directly. However, in the bulk, where this quantity is measurable, the dependence of the crystalline layer thickness on x_b is known to be nonlinear and is better approximated by a second-order polynomial [13,23], akin to Eq. (2).

The $d(\phi)$ curves calculated from Eq. (2) are shown in dash (hydrated) dash-dot-dotted (dry) lines for the four mixtures in Fig. 6. Equation (2) agrees better with the measurements for large-$\Delta n/\bar{n}$ mixtures than the linear approximation in Eq. (1), but now the deviations become larger for the small-$\Delta n/\bar{n}$ mixtures, e.g., Fig. 6(b).

C. In-plane structure

The GID measurements show an hexagonal in-plane packing for all alcohol mixtures studied, with a characteristic single GID diffraction peak at $q_r \approx 1.5$ Å^{-1}. The corresponding BRs show a surface-normal orientation of the bilayers' molecules, to within the experimental resolution of 4°–5° for all mixtures studied.

1. Lattice constant

The lattice spacings derived from the GID measurements are plotted in Fig. 7 for both the dry (open symbols) and the wet mixtures (solid symbols). As found earlier for pure alcohols [6], the in-plane lattice constant $a=2\pi/[q_r\cos 30°]$ (for a hexagonal cell) increases upon hydration. This is

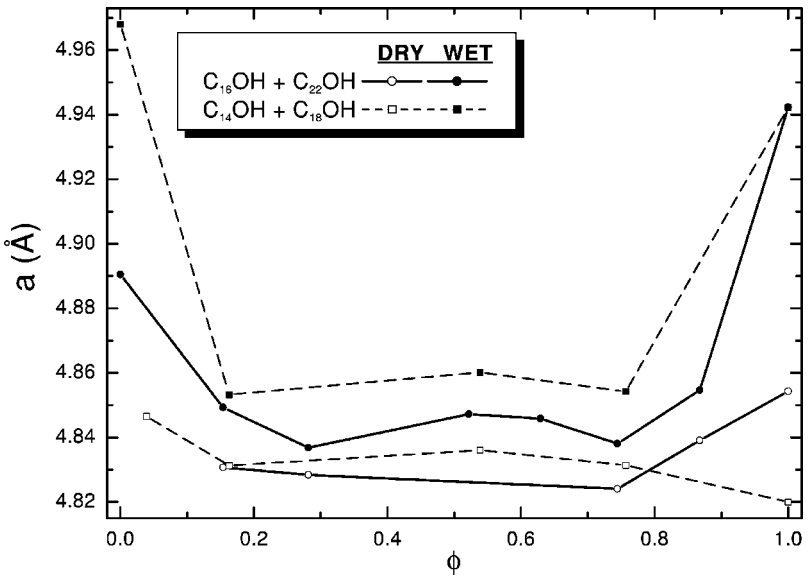

FIG. 7. The lattice constant $a(\phi)$ of the hexagonally packed surface-frozen bilayer, for several dry (open) and wet (solid) mixtures. While in the dry mixtures the lattice constant is almost independent of ϕ, the hydrated samples show significantly lower a values for the mixtures, compared to the pure materials. This effect may result from the existence of voids within the bilayer because of the close packing of different-length chains. The voids may facilitate the inclusion of water molecules in the layer without requiring a lattice expansion. The lines are only guides to the eye.

clearly observed in comparing the relevant $\phi=0$ and $\phi=1$ values in Fig. 7. Since the SF existence ranges ΔT for pure dry $C_{14}OH$ is zero and is very small for $C_{16}OH$, no in-plane data could be obtained for them at $\phi=0$. The most outstanding feature observed for the hydrated mixtures is the strong reduction in a, relative to the pure materials, for almost the full $0<\phi<1$ range. The increase in a upon hydration in pure alcohols most probably reflects the difficulty in incorporating the water molecules into the well-ordered, densely packed lattice having relatively few defects. By contrast, in mixtures the packing of two different chain lengths into the same crystalline structure should significantly increase the number of defects and voids, making possible the incorporation of water molecules into the structure without requiring a lattice dilation. Therefore, almost no difference is found between the lattice constants of a given mixture in its dry and wet states while for the pure materials the difference is large. In mixtures with a large chain length mismatch, $\Delta n/\bar{n}\gtrsim 0.35$, the lattice constant of the surface-frozen layer, a, at $\phi \in [0.25,0.5]$ is significantly lower than all the results obtained for small-$\Delta n/\bar{n}$ mixtures. In such mixtures, no significant mixing occurs at $\phi\gtrsim 0.25$, i.e., the surface bilayer consists of an almost pure long component as expected, and indeed found [18], for a solution of the long component in an inert solvent. In this case the usual linear thermal expansion of the SF layer results in a smaller a since the SF temperatures are reduced considerably from that of the pure solute's melt. Such a contraction of the lattice constant should be linear in T, allowing a measurement of the expansion coefficient of the SF bilayer as $\alpha_T=(da/dT)/a$, whenever a large existence range ΔT is obtained for a mixture. Unfortunately, the occurrence of black holes in the SF range of large-$\Delta n/\bar{n}$ mixtures limits the range of ϕ and the number of mixtures for which such measurements could be carried out.

In several samples the SF existence range ΔT was large enough (several degrees Celsius) to allow a measurement of the linear expansion α_T, at a constant bulk fraction ϕ. The results are listed in Table II. No specific n-dependent trend could be observed in the data. Very close values, $(1.02\pm0.05)\times10^{-3}\,^{\circ}C^{-1}$ (dry) and $(1.16\pm0.17)\times10^{-3}\,^{\circ}C^{-1}$ (wet) were measured recently for the $C_{14}OH+C_{18}OH$ alcohol mixtures [15]. The values in Table II are also close to the $(6\pm0.5)\times10^{-4}\,^{\circ}C^{-1}$ obtained for the dry and hydrated R_{II} bulk phase in pure and mixed alcohols [21], to the $(6.5\pm0.5)\times10^{-4}\,^{\circ}C^{-1}$ measured for a surface-frozen C_{23} alkane monolayer in a $C_{23}+C_{12}$ solution [18], and to the $(9\pm0.5)\times10^{-4}\,^{\circ}C^{-1}$ measured for the surface-frozen monolayer of a pure C_{20} alkane melt [24].

2. Molecular orientation

The orientation of the molecules relative to the surface normal can be determined from the measured BRs. Several typical measured BRs are shown in Fig. 8 for dry $C_{18}OH+C_{22}OH$ mixtures. A BR measured for a wet mixture is shown in the inset. The measured values (points) were fitted (lines) by the BR model used for dry and hydrated pure alcohols [6]. The model assumes a bilayer structure of hexagonally packed molecules, with the molecules of the upper layer residing in the hollows of the lower layer hexagons and taking into account that two equal-probability arrangements of this kind are possible [6,25]. The bilayer thickness and the roughness values obtained from the BR fits were found to agree in all cases with those refined from the XR measurement to within the combined error bars. The fits yield un-

TABLE II. The thermal expansion coefficient, $\alpha_T=(da/dT)/a$ of the lattice constant, a of the quasi-2D surface-frozen bilayer for the indicated C_mOH+C_nOH mixtures. ϕ is the liquid mole fraction of the longer component.

		Dry		Wet	
m	n	ϕ	α_T $(\times10^{-3}\,^{\circ}C^{-1})$	ϕ	α_T $(\times10^{-3}\,^{\circ}C^{-1})$
16	22	0.15	1	0.15	0.91
18	26	0.23	1.3	0.5	1.4
18	22	0.26	1.15		

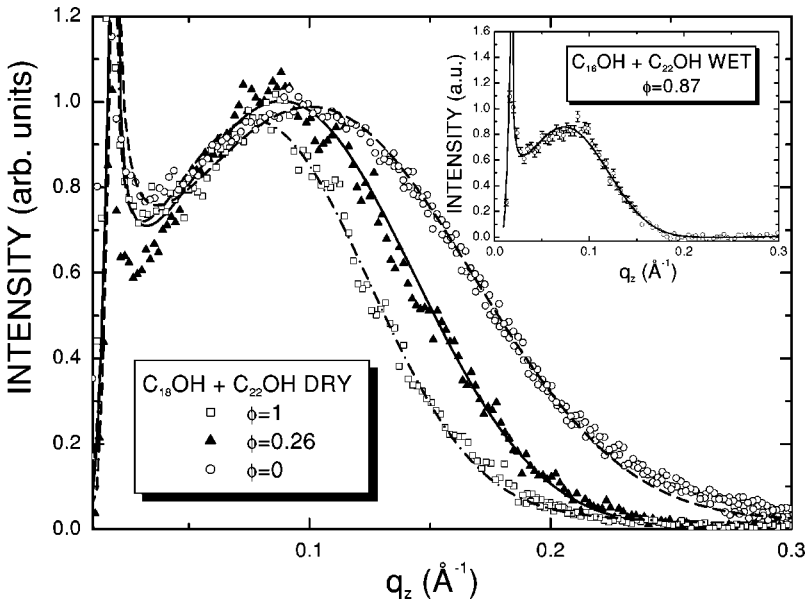

FIG. 8. Bragg rod scans for a series of $C_{18}OH+C_{22}OH$ dry mixtures (points). The width of the BR, which is inversely proportional to the surface-frozen bilayer's thickness, decreases with increasing ϕ. The corresponding growth of the bilayer thickness is due to the increase in the fraction of the long-chain molecules in the solid bilayer. The theoretical fits are shown (lines) to correspond well to the experimental data, except for the low-q_z region, $q_z \approx 0.03$ Å^{-1}, where the dip of the measured intensity is larger than that obtained from our model fit. The inset shows a representative Bragg rod scan for a hydrated alcohol mixture.

tilted molecules for all mixtures to within the $4-5°$ resolution of the experiment. This is unlike the SF bilayers of pure alcohols, where for $24 \leqslant n \leqslant 28$ tilted phases were observed [6]. The fact that even a small bulk admixture of a different-length alcohol eliminates the molecular tilt indicates that even in systems with very high chain length mismatch, a finite, though small, mixing of the two components occurs in the surface-frozen phase. It is also the case that a small amount of mixing eliminates the tilted phase in bulk alkanes. Future studies of the molecular orientation in mixtures of $24 \leqslant n \leqslant 28$ alcohol molecules at small bulk dilutions may reveal concentration-induced or temperature-induced tilting transitions. The BR's width is inversely proportional to the bilayer thickness. As shown in Fig. 8, the BR's width increases upon a reduction of ϕ, indicating a decrease in the bilayer thickness with an increase in the short component's concentration. In most of the dry mixtures, a small, but measurable, deviation of the theoretical fit from the experimental data is observed at low-q_z values, just above the strong Vineyard peak [26] at $q_z = q_c$, where $q_c \approx 0.02$ Å^{-1} is the surface-normal momentum transfer at the critical angle for total reflection. The experimental data in this region show a deep minimum which was not observed in pure materials and which could not be reproduced by the present model. While the origin of this feature is not clear, over the rest of the q_z range of the BR, the measured and fitted curves agree very well with each other, and the values refined from the fit agree well with those obtained from XR.

V. HYDRATION INDUCED TRANSITIONS

We now explore the effects of hydration in some detail. Though the expressions used for the hydrated and the non-hydrated mixtures are the same, the T_s values of the pure hydrated components are different from those of the dry ones [6,5]. Moreover, the ω_s values obtained from the fit of the theoretical expressions to the measured $T_s(\phi)$ are close to, but, usually, lower than those of the corresponding dry mixtures. In the small-$\Delta n/\bar{n}$ mixtures, the dry $x_s(\phi)$ curve almost coincides with the wet one [15], as shown for $C_{18}OH + C_{22}OH$ in Fig. 9 in dash-dotted (hydrated) and dash-dot-dotted (dry) lines. For large-$\Delta n/\bar{n}$ mixtures, the curvature of $x_s(\phi)$ is larger and so is the difference between the dry and the wet curves, as shown for dry (solid line) and wet (dashed line) $C_{18}OH+C_{26}OH$ in Fig. 9. We have denoted the x_s difference between dry and wet samples for these two mixtures by η and ε at particular concentrations, as marked in the figure.

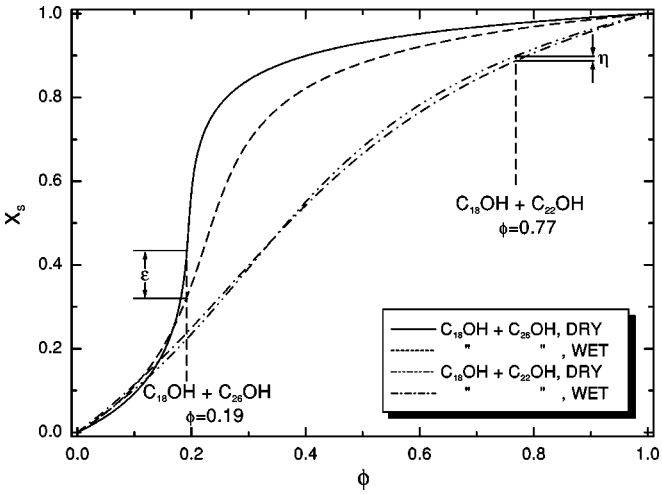

FIG. 9. The effect of hydration on the surface-frozen phase composition for the low- and the high-$\Delta n/\bar{n}$ limit. For small-chain length mismatch, the hydration changes only marginally the surface-frozen mole fraction x_s calculated from our theoretical model, as described in the text. See, e.g., the small difference η between the dry (dash-dot-dot) and the wet (dash-dot) $C_{18}OH + C_{22}OH$ surface-frozen fractions at $\phi = 0.77$. However, a significant change occurs upon hydration at the high-$\Delta n/\bar{n}$ limit: e.g., ε for the $C_{18}OH+C_{26}OH$ mixtures at $\phi = 0.19$ (solid and dashed line for dry and wet mixtures, respectively).

What would be the effect of these x_s differences on the measured layer thickness d? For the small-$\Delta n/\overline{n}$ limit, the x_s difference is negligible. Thus, the layer thickness will increase upon hydration only by the same ~ 2.5 Å found in pure alcohols and assigned to the intercalation of the water molecules into the bilayer's center [6]. In large-n pure alcohols, hydration may increase d by reducing the tilt angle. In the case of Fig. 9 this does not occur since no tilted phase is observed in these mixtures even when dry. In contrast to this simple behavior for small-$\Delta n/\overline{n}$ mixtures, the behavior of large-$\Delta n/\overline{n}$ mixtures is considerably more complicated. Here the molar concentration of the longer component, x_s, is significantly reduced upon hydration, as demonstrated by ε in Fig. 9. This drives a decrease in d, by an amount corresponding to the $x_s(\phi)$ difference. The intercalation, however, contributes to a fixed ~ 2.5 Å increase in d, as for small-$\Delta n/\overline{n}$ mixtures and pure compounds. The end result depends on the relative magnitudes of the two effects. The XR measurements, and the density profiles extracted therefrom, for the two samples discussed above, are shown in Fig. 10. The agreement with the trends discussed is very good. While for the $C_{18}OH+C_{22}OH$, $\phi=0.77$ mixture, the modulation period is reduced by hydration, indicating an increase in d, the opposite is found for the $C_{18}OH+C_{26}OH$, $\phi=0.19$ mixture. Here the modulation period increases upon hydration, indicating a decrease in thickness. This can be assigned to the dominance of the thickness decrease due to the reduction in x_s over the thickness increase due to the water intercalation. For a quantitative analysis, the four-slab electron density model discussed above was used, and fits (lines) to the measured (points) Fresnel-normalized XR were carried out. The resultant electron density profiles in Fig. 10(b) show the clear reduction of the layer thickness upon hydration in $C_{18}OH+C_{26}OH$, as expected from the reduced x_s derived from the $T_s(\phi)$-fitted curves in Fig. 9. The increase in the layer thickness of $C_{18}OH+C_{22}OH$ by ~ 2.5 Å is also clearly observed in the profiles plotted in Fig. 10(b).

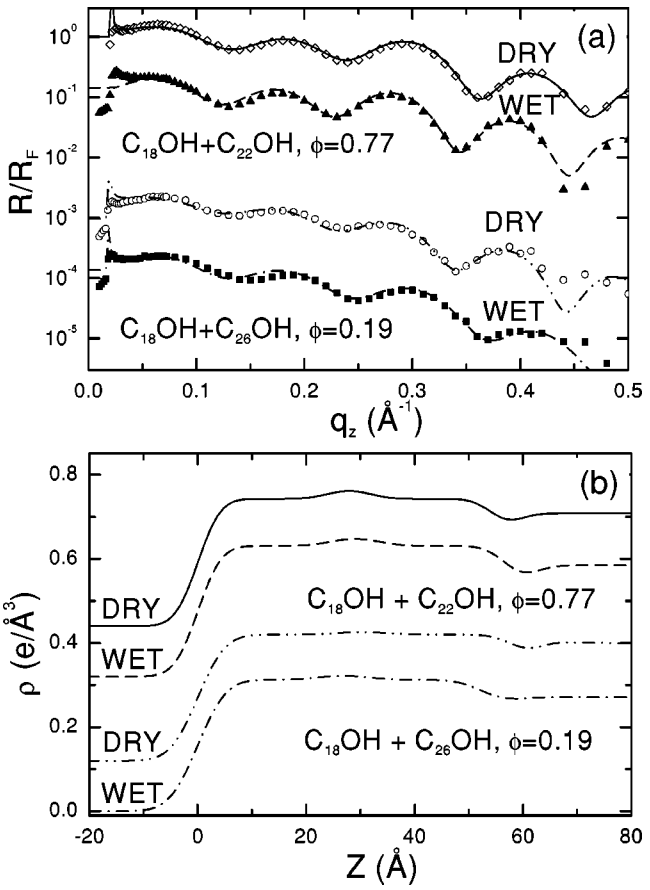

FIG. 10. (a) X-ray reflectivities (points) normalized to the Fresnel reflectivity of an ideally sharp interface, for the mixtures shown in Fig. 9. For $C_{18}OH+C_{22}OH$, $\phi=0.77$ the Kiessig fringes' period decreases upon hydration. This corresponds to an increase of ≈ 2.5 Å in the bilayer thickness, due to the intercalation of water molecules at the bilayer's center. The long component's mole fraction, x_s in the surface-frozen phase stays almost unchanged upon hydration from that of the bulk liquid fraction ϕ. By contrast, for $C_{18}OH+C_{26}OH$, $\phi=0.19$, the surface-frozen bilayer becomes considerably thinner upon hydration, even though water still intercalates into the bilayer's center. This is due to the fraction of the longer component incorporated into the surface-frozen bilayer being significantly reduced in the hydrated bilayer. The lines are fits of a four-slab model, as explained in the text. The surface-normal electron density profiles derived from the fit are shown in (b). Curves in (a) and (b) are shifted vertically for clarity.

VI. THE UNIVERSAL BEHAVIOR OF THE INTERCHANGE ENERGY

The interchange energy at the surface, ω_s, deduced from the fits of the theory to $T_s(\phi)$ for the dry (circles) and hydrated (squares) alcohol mixtures, is plotted in Fig. 11(a) as a function of the relative length mismatch squared, $(\Delta n/\overline{n})^2$. A linear dependence, albeit with some scatter, is evident. A fit (line) to all points yields $\omega_s/k_BT=12.1\times(\Delta n/\overline{n})^2$. The most striking result, however, is that all ω_s values, including the present results for dry and wet alcohol mixtures and those of the protonated-protonated and the deuterated-protonated alkane mixtures in Paper I, fall on the same line when plotted against $(\Delta n/\overline{n})^2$, as shown in Fig. 11(b). A fit to all points yields $\omega_s/k_BT=11.6\times(\Delta n/\overline{n})^2$ (solid line). An even better fit could be obtained by including only points with $(\Delta n/\overline{n})^2 \lesssim 0.12$. The fact that a universal behavior is observed indicates that the length-mismatch repulsion energy of the chains dominates over any other interaction present in the SF layer, e.g., HB in alcohols or the isotope mismatch repulsion in the deuterated-protonated alkanes. Moreover, the bulk interchange energy in alkanes and deuterated alkanes was also shown in Paper I to depend linearly on $(\Delta n/\overline{n})^2$, albeit with a higher prefactor: $\omega_b/k_BT=17.8\times(\Delta n/\overline{n})^2$. The higher bulk prefactor was assigned in Paper I to the more severe restrictions imposed on the packing of the molecules by the 3D bulk as compared to the 2D surface. In Fig. 12, we plot the bulk data and linear fit for alkanes from Paper I, along with the ω_b/k_BT values obtained here for hydrated alcohol mixtures. The good agreement of the present bulk hydrated alcohol results with the linear behavior of the alkane mixtures is clearly observed, even at

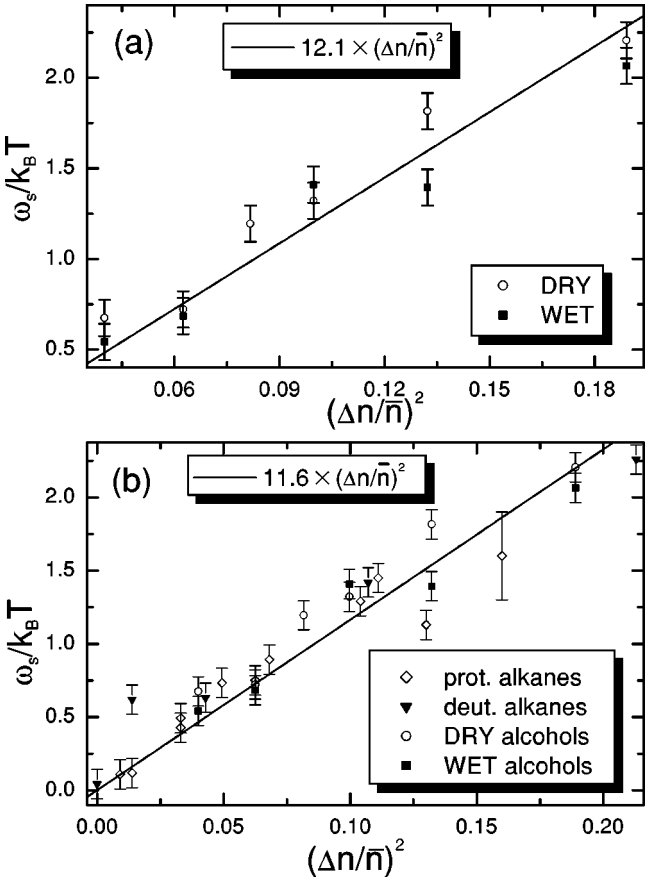

FIG. 11. (a) The interchange energy at the surface, ω_s, for the dry (open circles) and the wet (solid squares) surface-frozen phases. All alcohol results show a linear dependence on $(\Delta n/\bar{n})^2$. (b) The same as (a), but for all results measured for mixtures, including the protonated-protonated (open diamond) and the protonated-deuterated (solid triangle) alkane mixtures discussed in Paper I and the wet and dry alcohol mixtures addressed in this paper. Note the universal linear dependence observed. This behavior is rather striking, considering that in addition to the van der Waals interaction of simple alkanes, some of the samples interact also by hydrogen bonding (alcohols), or by isotopic repulsion (protonated-deuterated alkane mixtures).

considerably larger $(\Delta n/\bar{n})^2$ values than those of the alkane mixtures.

The microscopic origin of the repulsion energy is not clearly understood. Matheson and Smith [27] assign it, in bulk alkane mixtures, to the local lattice deformations needed to maintain continuity in a crystal comprising different-length molecules. The expression they obtain for the resultant repulsion energy seems, however, to depend linearly on $\Delta n/\bar{n}$, rather than the quadratic dependence observed here. Moreover, this theory may not be directly applicable to the SF bilayer, since the interlayer coupling, which plays an important role in the bulk, does not exist for the single surface-frozen layer. The repulsion energy could also be due to the smaller number of vdW contacts between, e.g., adjacent short-long molecules as compared to long-long ones. However, simple model calculations [28] of this effect yield results which should depend only on Δn, and overestimate the $\omega_{s,b}$ values extracted from our measurements by almost an order of magnitude. Clearly, a more sophisticated calculation is required, taking into account the likely presence of voids, gauche kinks, short-range clustering of equal-length molecules, etc., all of which contribute to the contact loss balance. An iron-clad justification for the linearity of $\omega_{s,b}$ in $(\Delta n/\bar{n})^2$ is therefore missing, though some explanation was provided also in Paper I. Theoretical work on this fundamental issue is clearly called for.

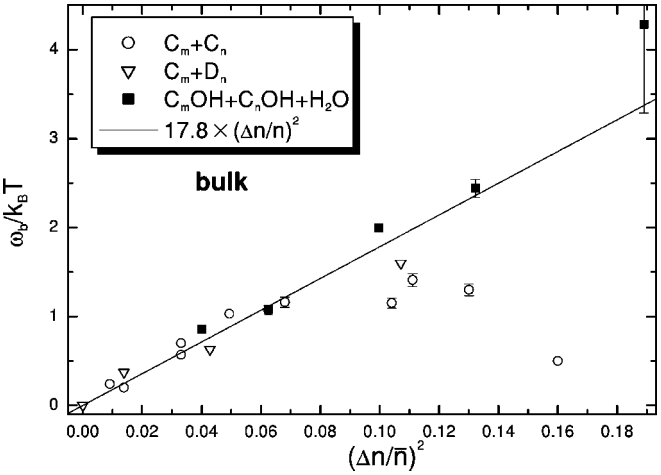

FIG. 12. Same as Fig. 11(b), but for the bulk. Note that the line is not a fit to all data points but the same line, which is representing the bulk alkane data in Paper I. Nevertheless, it agrees very well with all points measured for hydrated alcohols (solid squares).

VII. CONCLUSIONS

Surface freezing was studied here for binary mixtures of medium-length alcohols. In the present study only the even-even alcohol mixtures were considered, though it is possible that the odd-even and perhaps odd-odd mixtures may also show this effect. However, the simplicity of the even-even mixtures, which allow a theoretical description of the mixture based on the properties of the same effect in pure components led us to investigate those first.

The SF layer was found to consist of a bilayer with all hydroxyl groups residing at its center, as found for pure, monocomponent alcohols. No tilted phases were observed in any of the mixtures studied, even when one of the components exhibits such a phase when pure. For small relative length differences $\Delta n/\bar{n}$ the crystalline surface bilayer consists of a mixture of the two components, with a concentration close to that of the bulk. For large $\Delta n/\bar{n}$, the crystalline surface bilayer is strongly enriched by one of the components. In this case, the surface crystal was observed to undergo, at a specific (T,ϕ) point of a $C_{18}OH+C_{28}OH$ mixture, a solid-solid demixing phase transition [13]. The lattice constant of the surface-frozen layer in the mixtures studied was observed to behave qualitatively differently in the dry and the wet mixtures. In dry mixtures the lattice constants of the pure components and the mixtures are close. Upon hydration, however, a large increase in the pure components' lattice constants is observed, while only a small increase oc-

curs in the lattice constants of the mixtures. This effect was attributed to the presence of more voids and defects in the surface-frozen bilayer of mixtures than in those of the pure components, rendering the incorporation of water molecules into the surface-frozen bilayer of mixtures possible without increasing the interchain spacing. The linear expansion coefficient was measured for several mixtures, and found to be roughly the same as that published recently for a few other surface-frozen mono-component and bi-component samples, and also comparable to bulk values. The overall phase behavior of the mixtures, including the transition temperatures, the entropies, the bilayer thicknesses, the surface and bulk compositions, and the variation of all of these with $\Delta n/\overline{n}$, were quantitatively accounted for by the same theoretical model used for alkane mixtures in Paper I. The model contains only a single adjustable parameter, the interchange energy $\omega_{s,b}$. This parameter is found to be proportional to $(\Delta n/\overline{n})^2$, thus demonstrating a single, universal behavior, encompassing dry and hydrated alcohols and protonated-protonated and protonated-deuterated alkane mixtures. The exact microscopic origin of the interchange energy term $\omega_{s,b}$ is still unclear, as is its linear dependence on $(\Delta n/\overline{n})^2$. The mole fraction of the longer component in the SF layer, x_s, which is obtained from the theoretical fit to the measured $T_s(\phi)$ is a quantity which could perhaps be measured directly by atom-specific techniques, e.g., neutron reflectivity in deuterated-protonated mixtures. Such studies could distinguish not only between the linear and quadratic interpolation for $d(\phi)$, but may also reveal possible microphase separation in the quasi-2D surface-frozen layer, and, perhaps even possible superlattices of (or spatial lattice constant variations due to) different-length molecules in the layer. In addition to elucidating the structure of the surface-frozen phase in mixtures, this could also shed important light on the origins of the exchange energy $\omega_{s,b}$, which plays an important role in the phase behavior of both the bulk and the surface solid phases, and on its apparent universal linear $(\Delta n/\overline{n})^2$ dependence.

ACKNOWLEDGMENTS

We acknowledge the NSLS for beam time at X22B. Brookhaven National Laboratory is supported by the U.S. Department of Energy under Contract No. DE-AC02-98CH10886.

APPENDIX: MIXTURE THEORY FOR HYDRATED ALCOHOLS

First, consider an C_nOH+C_mOH alcohol mixture in its molten, liquid state. The number of $C_{n,m}OH$ molecules is N,M. Denote the number of water molecules absorbed by this mixture at saturation by $W=W(\phi)$, where $\phi=N/(N+M)$.

Similar to Eq. (4) in Paper I the free energy of this ternary mixture $C_nOH+C_mOH+H_2O$ can be written as

$$F_{\mathrm{III}}=Nf_n+Mf_m+Wf_w+k_BT\{N\ln[N/(N+M+W)]+M\ln[M/(N+M+W)]+W\ln[W/(N+M+W)]\}, \tag{A1}$$

where f_w is the free energy of the water molecule, $f_{m,n}$—those of *dry* $C_{m,n}OH$ molecules, and the term multiplied by k_BT is the mixing entropy of the ternary mixture, obtained by using the Stirling formula for $F=-kT\ln\Omega$, where $\Omega=(N+M+W)!/(N!M!W!)$.

Denote the number of water molecules that can be absorbed at saturation by $N(M)$ molecules of $C_nOH(C_mOH)$ by $NH_n(MH_m)$. The corresponding molar fractions of water are then $\phi_w^{n,m}=H_{n,m}/(1+H_{n,m})$. The $\phi_w^{n,m}$ values for the bulk and the surface of pure alcohols were published [6] as $\phi_{w,b}^n=0.663-0.1911\ln(n)$ and $\phi_{w,s}^n=0.1-3.23\times10^{-3}n$, respectively, in the n range discussed here. Thus, the free energy of N hydrated C_nOH molecules is

$$F_n=Nf_n+H_nNf_w+k_BT\{N\ln[(1+H_n)^{-1}]+NH_n\ln[H_n/(1+H_n)]\}. \tag{A2}$$

A similar expression can be written for the hydrated C_mOH. In the calculations in this paper we used for the hydrated alcohol mixtures a *binary* mixture formalism, Eq. (4) in Paper I, with values of *hydrated* pure alcohol free energies: $f_{n,m}^{lb}$ for the bulk and $f_{n,m}^{ls}$ for the surface. However, the *hydrated* pure alcohol free energy Nf_n^l is, by definition, the free energy of the C_nOH+H_2O mixture, given in Eq. (A2). We, substitute, therefore, Eq. (A2) explicitly into Eq. (4) in Paper I, and obtain

$$\begin{aligned}F^l=&\{Nf_n+H_nNf_w+k_BT[N\ln(1+H_n)^{-1}\\&+NH_n\ln\{H_n/(1+H_n)\}]\}+\{Mf_m+H_mMf_w\\&+k_BT[M\ln(1+H_m)^{-1}+MH_m\ln\{H_m/(1+H_m)\}]\}\\&+k_BT[N\ln\{N/(N+M)\}+M\ln\{M/(N+M)\}].\end{aligned} \tag{A3}$$

The indices b and s were omitted from this expression since it is valid for both the surface and the bulk.

We now calculate the difference, $\tau=F_{\mathrm{III}}-F^l$, between the rigorous expression for the free energy [Eq. (A1)] and the approximation used in this paper, Eq. (4) in Paper I or Eq. (A3). τ is the correction which should be inserted in our equations for $T_s(\phi)$ to take the hydration into account rigorously. Up to the first order in ϕ, W is

$$W=NH_n+MH_m. \tag{A4}$$

This means that the hydrated mixture is just a ϕ-weighted average between its pure components, and

$$\begin{aligned}(k_BT)^{-1}\tau=&\{N[\ln\{N/(N+M+W)\}-\ln(1+H_n)^{-1}\\&-\ln\{N/(N+M)\}]\}+\{M[\ln\{M/(N+M+W)\}\\&-\ln(1+H_m)^{-1}-\ln\{M/(N+M)\}]\}\\&+\{W\ln[W/(N+M+W)]-NH_n\\&\times\ln[H_n/(1+H_n)]-MH_m\\&\times\ln[H_m/(1+H_m)]\}.\end{aligned} \tag{A5}$$

Thus, the correction τ includes only an entropic part, which appears because of the indistinguishability of the water molecules absorbed in the C_nOH and in the C_mOH systems. In other words, τ is just the correction for the well-known Gibbs paradox [29]. Using Eq. (A4), the first curly bracket term in Eq. (A5) yields $N\ln[1+M(H_n-H_m)/(N+M+W)]$. Since $[M/(N+M+W)](H_n-H_m)\ll 1$, a first-order expansion yields: $N\ln[1+M(H_n-H_m)/(N+M+W)]\approx NM(H_n-H_m)/(N+M+W)$. The second curly bracket term yields by the same process the same result but with a negative sign, and thus the first two terms in Eq. (A5) cancel each other to a first approximation. Using Eq. (A4) in the third curly bracket term brings Eq. (A5) to the form

$$
\begin{aligned}
&(k_BT)^{-1}\tau \\
&\quad = MH_m\ln\{[NH_n/H_m+M]/ \\
&\qquad [N(1+H_n)/(1+H_m)+M]\}+NH_n \\
&\qquad \times\ln\{[N+MH_m/H_n]/[N+M(1+H_m)/(1+H_n)]\}.
\end{aligned}
\tag{A6}
$$

This expression can be included in our *binary* mixture free energy expression [Eq. (4) in Paper I], which is then differentiated with respect to N and M to yield the corresponding chemical potentials. Denoting $\alpha=N/M$, the derivatives of our correction are

$$
\begin{aligned}
&\tilde{\tau}_N\equiv(k_BT)^{-1}(\partial\tau/\partial N) \\
&\quad =[H_n-H_m]/[\alpha(1+H_n)+(1+H_m)] \\
&\qquad +H_n\ln\{[\alpha+H_m/H_n]/[\alpha+(1+H_m)/(1+H_n)]\},
\end{aligned}
$$

$$
\begin{aligned}
&\tilde{\tau}_M\equiv(k_BT)^{-1}(\partial\tau/\partial M) \\
&\quad =[H_m-H_n]/[\alpha^{-1}(1+H_m)+(1+H_n)]+H_m \\
&\qquad \times\ln\{[\alpha^{-1}+H_n/H_m]/[\alpha^{-1}+(1+H_n)/(1+H_m)]\}.
\end{aligned}
\tag{A7}
$$

Note that since the mixing of water molecules is random only in the liquid phase of the mixture, while in the solid (rotator) phase the H_2O molecules are restricted to the midbilayer region [6], no correction for indistinguishability is needed in the solid phase, since in all three mixtures, the C_nOH+H_2O, the C_mOH+H_2O, and the ternary $C_nOH+C_mOH+H_2O$, the mixing entropy of water should be zero. Including the corrections in Eq. (A7) in Eq. (8) in Paper I for the bulk freezing temperatures of the mixtures, $T_f(\phi)$, we finally obtain

$$
\begin{aligned}
T_f(\phi) &= [T_{f,n}\Delta S_n^b-\omega_b(1-x_b)^2]/[\Delta S_n^b+k_B\{\ln(x_b/\phi) \\
&\qquad -\tilde{\tau}_N\}], \\
T_f(\phi) &= [T_{f,m}\Delta S_m^b-\omega_b x_b^2]/[\Delta S_m^b+k_B\{\ln[(1-x_b)/(1-\phi)] \\
&\qquad -\tilde{\tau}_M\}].
\end{aligned}
\tag{A8}
$$

It is important to note that no additional unknown parameters are introduced by applying the correction. Similar equations are obtained also for the surface phase, as discussed in Paper I. For all bulk mixtures studied, $k_B|\tilde{\tau}_N|, k_B|\tilde{\tau}_M| < 0.08k_B$. At the surface the corrections are even smaller: $k_B|\tilde{\tau}_N|, k_B|\tilde{\tau}_M| < 0.03k_B$. These values are negligible relative to the $\Delta S_m^b \approx 15k_B$ of all mixtures studied. Finally, to correct the entropy loss prediction $\Delta S(\phi)$ of hydrated mixtures, a term of τ/T [Eq. (A6)] should be added to the original expression [Eq. (14) in Paper I]. However, in this case as well, the correction, peaking at equimolar surface fractions, is negligible by several orders of magnitude in comparison with the other additive terms in the equation.

Based on the above, we conclude that using for the hydrated alcohol mixtures a binary mixture formalism, based on the thermodynamical quantities measured for the pure hydrated components, is a very good approximation at least for all mixtures addressed in this study.

[1] E. Sloutskin, X.Z. Wu, T.B. Peterson, O. Gang, B.M. Ocko, E.B. Sirota, and M. Deutsch, Phys. Rev. E **68**, 031605 (2003), preceding paper.

[2] B.M. Ocko, X.Z. Wu, E.B. Sirota, S.K. Sinha, O. Gang, and M. Deutsch, Phys. Rev. E **55**, 3164 (1997).

[3] X.Z. Wu, B.M. Ocko, E.B. Sirota, S.K. Sinha, M. Deutsch, B.H. Cao, and M.W. Kim, Science **261**, 1018 (1993).

[4] X.Z. Wu, E.B. Sirota, S.K. Sinha, B.M. Ocko, and M. Deutsch, Phys. Rev. Lett. **70**, 958 (1993).

[5] O. Gang, B.M. Ocko, X.Z. Wu, E.B. Sirota, and M. Deutsch, Phys. Rev. Lett. **80**, 1264 (1998).

[6] O. Gang, X.Z. Wu, B.M. Ocko, E.B. Sirota, and M. Deutsch, Phys. Rev. E **58**, 6086 (1998).

[7] O. Gang, B.M. Ocko, X.Z. Wu, E.B. Sirota, and M. Deutsch, Phys. Rev. Lett. **82**, 588 (1999).

[8] O. Gang, B.M. Ocko, X.Z. Wu, E.B. Sirota, and M. Deutsch, J. Phys.: Condens. Matter **12**, A357 (2000).

[9] A.V. Tkachenko and Y. Rabin, Phys. Rev. Lett. **76**, 2527 (1996).

[10] A.V. Tkachenko and Y. Rabin, Phys. Rev. E **55**, 778 (1997).

[11] E.B. Sirota, X.Z. Wu, B.M. Ocko, and M. Deutsch, Phys. Rev. Lett. **79**, 531 (1997); A.V. Tkachenko and Y. Rabin, *ibid.* **79**, 532 (1997).

[12] P.K. Mukherjee and M. Deutsch, Phys. Rev. E **61**, 637 (2000).

[13] E. Sloutskin, O. Gang, H. Kraack, M. Deutsch, B.M. Ocko, and E.B. Sirota, Phys. Rev. Lett. **89**, 065501 (2002).

[14] X.Z. Wu, B.M. Ocko, H. Tang, E.B. Sirota, S.K. Sinha, and M. Deutsch, Phys. Rev. Lett. **75**, 1332 (1995).

[15] E. Sloutskin, E.B. Sirota, H. Kraack, O. Gang, A. Döerr, B.M. Ocko, and M. Deutsch, J. Chem. Phys. **116**, 8056 (2002).

[16] J.H. Hildebrand and R.L. Scott, *The Solubility of Nonelectrolytes* (Reinhold, New York, 1950).

[17] E.A. Guggenheim, *Mixtures* (OUP, Oxford, 1952).
[18] E. Sloutskin, E.B. Sirota, H. Kraack, B.M. Ocko, and M. Deutsch, Phys. Rev. E **64**, 031708 (2001).
[19] E.B. Sirota, J. Chem. Phys. **112**, 492 (2000).
[20] H. Kraack, E.B. Sirota, and M. Deutsch, J. Chem. Phys. **112**, 15 (2000).
[21] E.B. Sirota and X.Z. Wu, J. Chem. Phys. **105**, 7763 (1996).
[22] S.S. Katti and S. Pathak, J. Chem. Eng. Data **14**, 73 (1969).
[23] S. Amelinckx, in *Proceedings of an International Conference on Crystal Growth, Cooperstown*, New York, 1958, edited by R.H. Doremus, B.W. Roberts, and D. Turnbull (Wiley, New York, 1958), pp. 586–592.
[24] B.M. Ocko *et al.*, Phys. Rev. E **63**, 032602 (2001).
[25] M. Deutsch, X.Z. Wu, E.B. Sirota, S.K. Sinha, B.M. Ocko, and O.M. Magnussen, Europhys. Lett. **30**, 283 (1995).
[26] G.H. Vineyard, Phys. Rev. B **26**, 4146 (1982).
[27] R.R. Matheson, Jr. and P. Smith, Polymer **26**, 288 (1985).
[28] E. Sloutskin *et al.* (unpublished).
[29] R.K. Pathria, *Statistical Mechanics*, 2nd ed. (Butterworth, Oxford, 1996), p. 22.